Proceedings of ASME Turbo Expo 2025
Turbomachinery Technical Conference and Exposition
GT2025
June 16-20, 2025, Memphis, Tennessee

GT2025-152452

AN EXTENDED ARTIFICIALLY THICKENED FLAME MODEL FOR TURBULENT HYDROGEN AND HYDROGEN-ENRICHED FLAMES WITH INTRINSIC INSTABILITIES UNDER GAS TURBINE RELEVANT CONDITIONS

Vinzenz Schuh[1,*], Driss Kaddar[1], Antonia Bähr[1], Mathis Bode[2], Christian Hasse[1], Hendrik Nicolai[1]

[1]Technical University of Darmstadt, Department of Mechanical Engineering, Simulation of Reactive Thermo-Fluid Systems, Otto-Berndt-Str. 2, 64287 Darmstadt, Germany
[2]Jülich Supercomputing Centre, Forschungszentrum Jülich GmbH, 52425 Jülich, Germany

ABSTRACT

Hydrogen and hydrogen-blends with ammonia or natural gas are cornerstones in the transition to future environmentally friendly energy systems, such as gas turbines and aero-engines. However, hydrogen's unique characteristics lead to intrinsic flame instabilities, resulting in an up to sixfold increase in turbulent flame speeds under gas turbine-relevant conditions compared to flames without instabilities. These effects are not captured by current combustion models, presenting a major barrier for Computational Fluid Dynamic simulations. This study addresses these limitations by developing an extension to the widely used Artificially Thickened Flame (ATF) model, validating it for wide operating conditions and applying it to turbulent configurations. To this extent, over 200 direct numerical simulations (DNS) of laminar planar flames are analyzed, unraveling the characteristics of the enhanced flame speed. The subsequently developed model is validated across comprehensive variations in pressure ($1\,\mathrm{atm} - 20\,\mathrm{atm}$), temperature ($300\,\mathrm{K} - 700\,\mathrm{K}$), equivalence ratios ($\Phi = 0.4 - 1.0$), and fuel compositions (pure H_2, pre-cracked ammonia ($NH_3/H_2/N_2$) and hydrogen natural gas blends (CH_4/H_2)) to ensure the model's applicability for technically relevant operating conditions. Additionally, the model is transferred to turbulent conditions using Large Eddy Simulations. For model validation, multiple high-fidelity DNS of turbulent jet flames at various conditions are performed. The advanced model shows excellent agreement in a laminar configuration and significant improvements in predicting turbulent flame speeds of the turbulent jet flames compared to the state-of-the-art model. By enhancing the widely used ATF model to account for hydrogen characteristics, this study supports the further development of efficient and environmentally friendly hydrogen-powered energy systems.

Keywords: Combustion, Modeling, Hydrogen, Hydrogen-Blends, Ammonia, Thickened Flame, Intrinsic Instabilities

*Corresponding author: schuh@stfs.tu-darmstadt.de

1. INTRODUCTION

Hydrogen is considered a promising energy carrier for the decarbonization of technical systems, especially in those with a high energy demand. In particular, thermochemical energy conversion is a powerful strategy for integrating hydrogen and hydrogen-blends into energy systems, such as aero-engines and stationary gas turbines. In this context, pure hydrogen H_2 as well as hydrogen blends with ammonia NH_3 and natural gas CH_4 are essential for ensuring compatibility and flexibility towards hydrogen-ready energy systems [1]. Rapidly adopting existing and developing new systems for a safe and efficient operation with hydrogen and hydrogen blends necessitates predictive reactive Computational Fluid Dynamic (CFD) simulations.

A key design aspect of new hydrogen combustion systems is limiting NOx emissions, making lean combustion a preferred approach. However, these conditions promote intrinsic flame instabilities arising from hydrogen's high diffusivity. These so-called thermo-diffusive (TD) instabilities lead to a manyfold increase of the flame speed due to enhanced flame wrinkling and local stratification. TD instabilities in hydrogen flames under ambient conditions have been shown to increase the flame speed up to four times the laminar burning velocity [2]. This effect becomes even more pronounced under practically relevant increased pressure conditions leading to up to six times higher flame speeds [3]. Instabilities have also proven highly significant in turbulent configurations, where markedly higher turbulent flame speeds have been reported [4]. The exact prediction of the turbulent flame speed and TD instabilities are crucial for the efficient and safe design of combustors, e.g., to prevent flashback. However, state-of-the-art combustion models disregard the impact of intrinsic instabilities, making CFD unreliable and creating a major roadblock in developing next-generation gas turbine technologies.

As a first step to overcome this, we recently extended the Artificially Thickened Flame (ATF) approach, also called Thickened Flame Model (TFM) [5] to account for TD instabilities,

demonstrating accurate predictions of enhanced flame speeds in laminar configurations under ambient conditions with simplified chemistry [5]. Given the strong dependence of TD instabilities on operating conditions like pressure, temperature, and fuel composition, this work takes the important follow-up step of extending the model to encompass a broad range of technically relevant conditions using detailed chemical kinetics. Furthermore, the model is extended to turbulent simulations and validated in a turbulent jet flame, using a set of high-fidelity turbulent DNS data that is created as part of this work. In summary, the objectives of this study are:

- Model generalization to technically relevant conditions including variations of:
  - Equivalence ratio: $\Phi = 0.4 - 1.0$
  - Preheating temperature: $T_\mathrm{u} = 300\,\mathrm{K} - 700\,\mathrm{K}$
  - Pressure: $p = 1\,\mathrm{atm} - 20\,\mathrm{atm}$
  - Fuel composition: H_2; CH_4-H_2; NH_3-H_2-N_2
- Extension to turbulent conditions
- Model evaluation using high-fidelity DNS data of turbulent jet flames under broad operating conditions

The remainder of the paper is structured as follows: The model development begins by outlining the theoretical background, revisiting key characteristics of thermodiffusive instabilities, and introducing the state-of-the-art ATF approach. This is followed by the derivation of the efficiency function for TD instabilities. The model coefficients are generalized using a normalization strategy covering the aforementioned parameter space. The effectiveness of the generalized model is showcased in a laminar configuration. The generalized model is then put to the test in a turbulent jet flame configuration for four different operating conditions, where its performance is rigorously evaluated against the high-fidelity DNS data.

2. THEORETICAL BACKGROUND

In this section, characteristics of TD instabilities in lean premixed hydrogen flames are recalled and the ATF approach is introduced.

2.1 Thermo-diffusive (TD) instabilities

In the following, key aspects of TD instabilities are recalled including characteristic quantities needed for the model development. Intrinsic TD instabilities can be observed in fuel-lean hydrogen/hydrogen-enriched combustion systems and have extensively been studied in the literature [2, 5–8]. These instabilities manifest when planar hydrogen flames become unstable leading to the formation of cellular and finger-like structures as well as local mixture stratification. TD instabilities arise from hydrogen's low Lewis number Le leading to differential diffusion, which results in a local focusing and defocusing effect of heat and local enrichment of hydrogen in regions of positively curved flame fronts along a deflected flame front [1].

Exemplary, a resulting TD unstable flame front is depicted in Fig. 1 by the temperature T normalized as $\Theta = (T - T_\mathrm{u})/(T_\mathrm{ad} - T_\mathrm{u})$ with T_u and T_ad as the unburned and adiabatic temperature at the given conditions. The normalized temperature is advantageous since values above unity indicate super-adiabatic temperatures resulting from the local fuel stratification. Additionally, various sized cellular and finger-like structures are visible. Here, a smallest and largest structure can be identified. The smallest structure is often characterized by the so-called critical wavelength λ_crit. It is the smallest instability structure and can be estimated using a linear stability analysis [2, 5]. The largest intrinsic structure $L_\mathrm{cell,max}$ is the maximum size, the instabilities grow before they interfere with other structures or break down into smaller cellular structures. In prior studies, Creta et al. [8, 9], identified $L_\mathrm{cell,max}$ to be approximately $30 \cdot \lambda_\mathrm{crit}$. The flame speed of an unstable flame is significantly affected by the size distribution of the cells in the flame front [3, 5]. To measure the flame speed, the fuel consumption speed of two-dimensional planar flames s_c is defined as the integral fuel source term $\dot{\omega}_\mathrm{fuel}$ normalized by the domain size L_y, the unburned density ρ_u and hydrogen mass fraction $Y_\mathrm{fuel,u}$:

$$s_\mathrm{c} = \frac{-1}{Y_\mathrm{fuel,u} \cdot \rho_\mathrm{u} \cdot L_y} \int \dot{\omega}_\mathrm{fuel} dx dy. \tag{1}$$

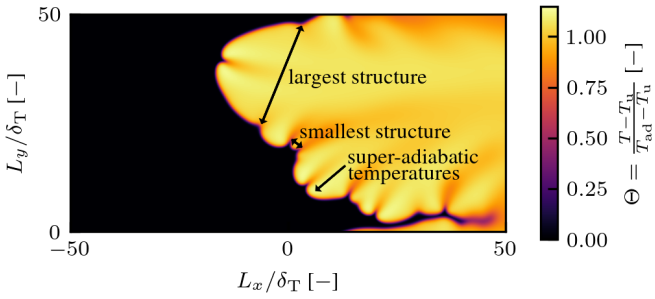

FIGURE 1: CONTOUR PLOT OF THE NORMALIZED TEMPERATURE $\Theta = (T - T_\mathrm{u})/(T_\mathrm{ad} - T_\mathrm{u})$ OF A FLAME FRONT WITH TD INSTABILITIES. REGIONS OF SUPER-ADIABATIC TEMPERATURES AS WELL AS THE SMALLEST AND LARGEST INSTABILITY STRUCTURES ARE MARKED.

2.2 Artificially Thickened Flame (ATF) model

The ATF model is a widely adopted turbulence-chemistry interaction model that artificially thickens the physical flame, lowering spatial resolution requirements in Large Eddy Simulations (LES). The thickening is achieved by a coordinate transformation maintaining the laminar flame speed s_l while broadening the flame thickness δ_T [10]. This is accomplished by scaling the diffusion velocity $V_{k,i}$ in the species and enthalpy transport equation by a thickening factor F, while dividing the corresponding source terms $\dot{\omega}_k$ by F [11]. The resulting transport equation, exemplary shown for the species mass fraction Y_k, reads:

$$\frac{\partial \rho Y_k}{\partial t} + \frac{\partial \rho u_i Y_k}{\partial x_i} = \frac{\partial}{\partial x_i}\left(F E_\mathrm{turb} \rho Y_k V_{k,i}\right) + \frac{E_\mathrm{turb} \dot{\omega}_k}{F}. \tag{2}$$

In turbulent flows, the flame's response to turbulence is reduced when applying this model. As a result, the flame becomes less wrinkled, leading to a smaller flame surface area and, consequently, a lower turbulent flame speed. To correct for this decreased flame surface, additional modeling is required. Charlette et al. [12] designed an efficiency function E_turb (already included

in Eq. (2)) to compensate for the weaker flame response and to increase the turbulent flame speed, which has been shown to be effective for hydrocarbon fuels [13].

Known limitations of the ATF approach are flame stretch and capturing the impact of thermodiffusive instabilities. Recent efforts have been focused on including stretch effects into the model [14–17]. A stretch-corrected approach is also adopted and applied for ammonia-hydrogen blends to a turbulent configuration in [18]. Schuh et al. [5] proposed an extension for laminar unstable flames using single-step chemistry which is the basis for the subsequent development.

3. MODEL DEVELOPMENT AND GENERALIZATION

Assessing and characterizing intrinsic TD instabilities as well as understanding their interaction with the ATF model is done using commonly employed laminar two-dimensional initially planar flames [2, 5, 6]. Accordingly, this configuration is considered here for model development and parameterization under various conditions.

3.1 Numerical setup

The computational domain is schematically shown in Fig. 2. The two-dimensional flames are initialized by one-dimensional flame profiles and disturbed by a sinusoidal perturbation with a small amplitude A_0. From this initial deflection, TD instabilities develop. It has been shown by Berger et al. [2] that the fully developed instabilities, which are the focus of this work, do not depend on the initial deflection. The flame is stabilized within the domain by dynamically matching the inlet velocity u_{in} to the effective flame speed s_c.

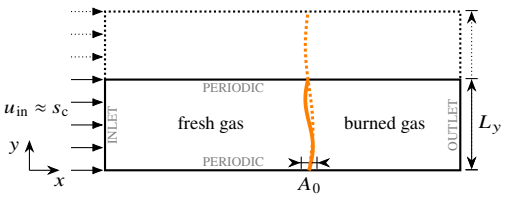

FIGURE 2: SCHEMATIC OF THE 2D COMPUTATIONAL DOMAIN. THE DOMAIN HEIGHT L_y IS VARIED AS INDICATED BY THE DOTTED LINES.

As shown in Fig. 1, instabilities comprise varying length scales from cellular structures to finger-like structures. To trigger varying instability structures and quantify the influence of different length scales on the flame speed, the domain size L_y is varied in the flame tangential direction as shown in Fig. 2 by the dotted lines. L_y is varied between $2\delta_T$ and $128\delta_T$, specifically taking the values $2\delta_T$, $4\delta_T$, $6\delta_T$, $8\delta_T$, $12\delta_T$, $16\delta_T$, $32\delta_T$, $64\delta_T$ and $128\delta_T$, where δ_T is the laminar flame thickness based on the maximum temperature gradient of the corresponding one-dimensional flame. The domain length L_x is set to be large enough to avoid an influence of the inlet and outlet on the flame propagation.

A well-validated solver based on OpenFOAM [5, 19] which includes the ATF model is used. The extensive parameter variation including gas turbine relevant conditions is performed with PeleLMeX [20] utilizing its adaptive mesh refinement (AMR) capabilities and, subsequently, reducing computational costs significantly. Both solvers assume ideal gas and employ the low Mach number assumption for the reactive Navier-Stokes equations using the Hirschfelder–Curtiss approximation for scalar diffusion velocity including thermo-diffusion [21]. A correction velocity for the species diffusion is employed to ensure mass conservation. The equations are spatially and temporally discretized using second-order schemes. A grid resolution of 26 (OpenFOAM) and 32 (PeleLMeX) grid points within the laminar flame thickness δ_T is employed, wherein PeleLMeX an AMR strategy following Howarth et al. [22] is utilized. Prior studies have shown that the chosen resolution is sufficient to correctly predict the flame properties of interest [2, 5].

For model development in Subsec. 3.3, the mechanism of Burke et al. [23] is utilized for the pure hydrogen cases. The methane-hydrogen cases employ the mechanism by Stagni et al. [24] while an ammonia-hydrogen mechanism by Stagni et al. [25] is used for the pre-cracked ammonia mixtures. To reduce computational costs, the mechanism by Smooke et al. [26] is taken for the methane-hydrogen case during model validation in the turbulent jet flame (cf. Subsec. 4.2). The turbulent hydrogen and ammonia-hydrogen cases are computed using the same mechanism as used during model development. All mechanisms are well-validated for the respective operating conditions.

3.2 Influence of flame thickening on TD instabilities

Fully developed intrinsic instabilities in a domain of size $L_y = 128\delta_T$ with varying thickening factors are shown in Fig. 3. The contour plots show the normalized temperature Θ. The left plot shows the result of the DNS ($F = 1$) while the middle and right contours show flames computed with increasing thickening factors F. All flames show similarly wrinkled flame fronts and similar super-adiabatic temperature regions ($\Theta > 1$) indicating TD instabilities. Additionally, similar to Fig. 1, smallest and largest structures can be identified in all contour plots of Fig. 3. However, the instability structures grow larger with increasing thickening factor. As demonstrated in our recent work [5], thickening does not suppress instabilities but alters the size of the intrinsic length scale of the instabilities. To be more specific, all instability structures, including the smallest λ_{crit} and largest instability structures $L_{\text{cell,max}}$, scale linearly with F. This effect is present regardless of the chemical modeling approach.

To quantify the influence of the thickening, the consumption speeds of the highly dynamic flames are averaged over time. After the instabilities are fully developed, $\langle s_c \rangle$ is averaged for a sufficiently long time, at least 100 flame times, where the flame time τ is defined as $\tau = \delta_T / s_l$ (see Tab. 1). The results are illustrated in Fig. 4, which shows the temporally averaged fuel consumption speed $\langle s_c \rangle$, normalized by the laminar flame speed s_l, for varying normalized domain sizes L_y and thickening factors F. The three lines correspond to various thickening factors $F = 1$ (reference DNS), $F = 2$ and $F = 4$ where each line consists of multiple simulations at varying domain sizes L_y. The average consumption speed of the flames shown in Fig. 3 correspond to the very right points in Fig. 4 ($L_y/\delta_T = 128$). Connecting the altered instability structures shown in Fig. 3 to the difference in averaged consumption speed in Fig. 4 for the different thickening factors, it becomes

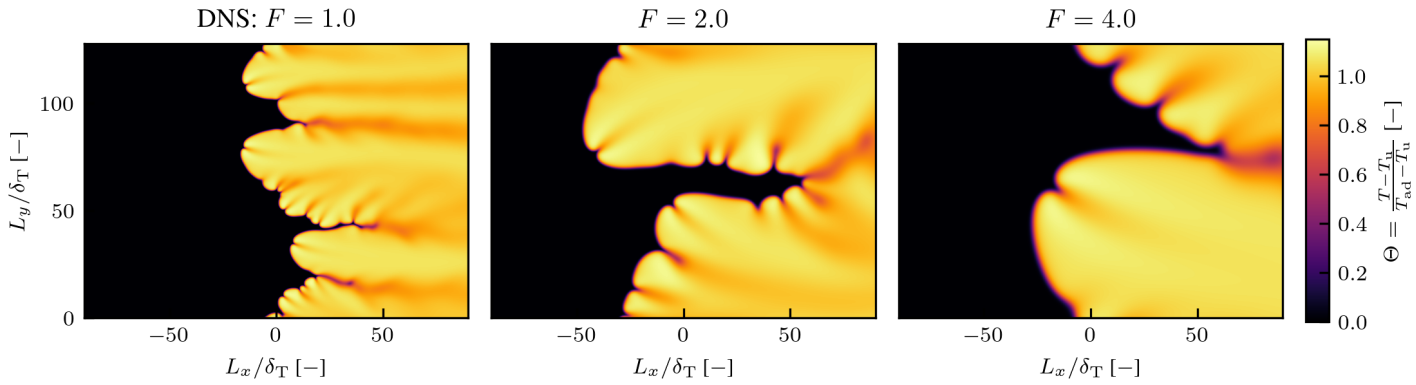

FIGURE 3: CONTOUR PLOTS OF THE NORMALIZED TEMPERATURE Θ SHOWING 2D FLAMES WITH INTRINSIC INSTABILITIES COMPUTED AS DNS ($F = 1$) AND WITH VARYING THICKENING FACTORS F AT AMBIENT CONDITIONS AND $\Phi = 0.4$. VALUES ABOVE UNITY INDICATE SUPER-ADIABATIC TEMPERATURES.

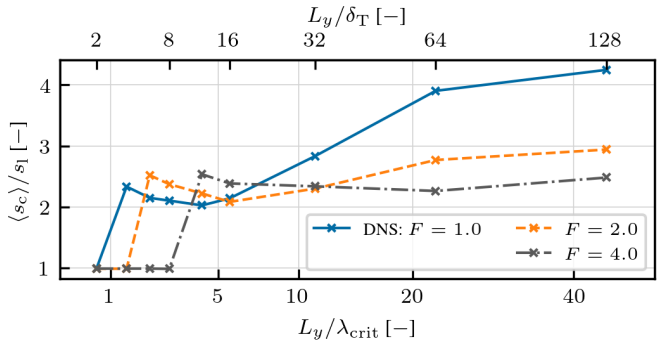

FIGURE 4: AVERAGED FUEL CONSUMPTION SPEED $\langle s_c \rangle$ NORMALIZED BY THE LAMINAR FLAME SPEED s_l PLOTTED OVER THE VARYING DOMAIN SIZES L_y AND FOR VARYING THICKENING FACTORS F.

clear that the scaled instability structures result in significantly different flame speeds. To clarify, the DNS shows that instabilities lead to a fourfold increase of s_c compared to s_l when the domain size is set to $L_y = 128\delta_T$ while the simulation with $F = 4$ predicts an increase of ~ 2.5, underlining that thickening strongly influences the consumption speed. The difference between $\langle s_c \rangle$ from the DNS ($F = 1$) and $\langle s_c \rangle$ from the simulations with ATF ($F \neq 1$) is to be predicted by the model extension. Consequently, the model must increase the flame speed by 60% for $L_y = 128\delta_T$ and $F = 4$.

Besides the influence of the thickening, Fig. 4 also shows that the domain size L_y is crucial for the observed consumption speed $\langle s_c \rangle$. In Fig. 4, the domain size L_y is shown on the x-axis and normalized in two different ways. On the top axis, the domain size L_y is normalized by the flame thickness δ_T. On the bottom x-axis, the domain size is normalized by the critical wavelength λ_{crit}, i.e., the smallest instability structure (cf. Subsec. 2.1). Therefore, the bottom x-axis represents how many of the smallest instability structures fit into the domain of a given size. As expected, when the domain is smaller than λ_{crit}, no increase ($\langle s_c \rangle / s_l = 1$) is visible since in these cases no instabilities are present. Besides the smallest instability structure λ_{crit}, also the largest instability structure $L_{cell,max}$ plays a role for the prediction of $\langle s_c \rangle$. As mentioned in Subsec. 2.1, no larger instability structures than $L_{cell,max}$ are present, with $L_{cell,max} \approx 30\lambda_{crit}$. Consequently, the instabilities are either limited by the domain size L_y or by the intrinsic size of the largest instability structure $L_{cell,max}$. Concluding, an upper length scale for the instability structures $\Delta = \min\left(L_y, L_{cell,max}\right)$ can be defined to be either limited by the domain size or the intrinsic upper cut-off. This upper length scale Δ, in turn, determines the flame consumption speed: $\langle s_c \rangle / s_l = f(\Delta)$. Similar to the instability structures themselves, the upper length scale Δ scales linearly with F, which implies that $f(\Delta)$ can be used to determine the flame speed for the thickened and non-thickened flame when scaled accordingly.

Since the model needs to predict the ratio between $(\langle s_c \rangle / s_l)|_{F=1}$ and $(\langle s_c \rangle / s_l)|_{F\neq 1}$ the efficiency function is defined as the ratio of $f(\Delta)$ to $f(\Delta/F)$:

$$E_{TD} = \frac{(\langle s_c \rangle / s_l)|_{F=1}}{(\langle s_c \rangle / s_l)|_{F\neq 1}} = \frac{f(\Delta)}{f(\Delta/F)}. \tag{3}$$

In summary, for a predictive ATF model, we require knowledge of the function $f(\Delta)$ determining the consumption speed $\langle s_c \rangle$ for all domain sizes, so that $f(\Delta)$ represents the blue curve ($F = 1$) in Fig. 4.

3.3 Generalization of the E_{TD} to various conditions

The dependency of $\langle s_c \rangle$ on the domain size for various operating conditions is investigated to derive a general formulation of $f(\Delta)$ in the following. Due to the characteristic smallest and largest instability length scales dictating the consumption speed, a fractal-like ansatz for the function f is considered:

$$f(\Delta) = 1 + \frac{\beta_1}{\mathscr{C}} \cdot \left(\frac{\Delta}{\lambda_{crit}}\right)^{\beta_2}, \tag{4}$$

where β_1 and β_2 and a normalization factor $\mathscr{C}$ are model parameters. Hereby, the normalization factor $\mathscr{C}$ and the smallest instability length scale λ_{crit} additionally depend on the operating

TABLE 1: OVERVIEW OF THE CONDITIONS CONSIDERED FOR MODEL DEVELOPMENT INCLUDING MIXTURE PROPERTIES AND FLAME CHARACTERISTICS OF CORRESPONDING ONE-DIMENSIONAL FREELY PROPAGATING FLAMES. FOR EACH CONDITION, NINE DIRECT NUMERICAL SIMULATIONS (DNS) WITH VARYING DOMAIN SIZES L_y ARE CONDUCTED.

fuel	$X_{H_2,\mathrm{fuel}}$ [%]	Φ [−]	p [atm]	T_u [K]	Le_{eff} [−]	σ [−]	Ze [−]	$\lambda_{\mathrm{Crit}}/\delta_T$ [−]	s_l [cm s^{-1}]	δ_T [µm]	τ [ms]
H2	1	0.40	1.0	300	0.34	4.42	11.56	2.85	21.26	651	3.07
H2	1	0.50	1.0	300	0.37	5.01	9.00	2.97	53.13	426	0.80
H2	1	0.50	5.0	300	0.35	5.01	12.91	2.88	24.33	114	0.47
H2	1	0.50	10.0	300	0.34	5.01	17.07	2.63	13.49	88	0.66
H2	1	0.50	1.0	500	0.39	3.31	5.87	2.97	201.16	433	0.22
H2	1	0.50	3.0	500	0.38	3.31	7.90	2.88	138.26	121	0.09
H2	1	0.50	1.0	700	0.43	2.58	3.41	2.63	536.44	509	0.10
H2	1	0.50	3.0	700	0.41	2.58	4.87	2.57	430.19	123	0.03
H2	1	0.50	10.0	700	0.38	2.59	7.37	2.93	245.11	31	0.01
H2	1	0.50	20.0	700	0.37	2.59	9.06	3.14	149.28	17	0.01
H2	1	0.65	1.0	300	0.43	5.76	6.69	2.85	114.98	356	0.31
H2	1	1.00	1.0	300	0.66	6.86	5.81	2.83	233.39	361	0.15
NH3-H2-N2	0.60	0.40	1.0	300	0.44	4.29	15.08	2.94	7.48	1327	17.74
NH3-H2-N2	0.75	0.40	1.0	300	0.40	4.28	11.48	2.82	20.33	666	3.28
NH3-H2-N2	0.30	0.80	1.0	300	0.56	6.19	7.77	4.35	16.14	873	5.41
NH3-H2-N2	0.45	0.80	1.0	300	0.56	6.19	7.77	4.21	33.04	530	1.60
NH3-H2-N2	0.60	0.80	1.0	300	0.56	6.19	7.77	3.37	66.03	398	0.60
NH3-H2-N2	0.75	0.80	1.0	300	0.55	6.05	5.71	2.99	145.97	361	0.25
CH4-H2	0.20	0.80	1.0	300	0.75	6.66	9.21	6.50	26.99	521	1.93
CH4-H2	0.40	0.80	1.0	300	0.63	6.63	9.01	5.67	32.37	466	1.44
CH4-H2	0.60	0.80	1.0	300	0.56	6.58	8.72	4.94	42.23	404	0.96
CH4-H2	0.80	0.80	1.0	300	0.51	6.51	8.19	4.07	65.54	339	0.52
CH4-H2	0.90	0.80	1.0	300	0.50	6.45	7.51	3.47	93.19	318	0.34

conditions and fuel composition. Therefore, λ_{crit} is computed using linear stability analyses [5] and tabulated in Tab. 1 while $\mathscr{C}$ will be determined in the following.

To determine the parameters in Eq. (4), a comprehensive variation of operating conditions and domain sizes is considered. The variation consists of an equivalence ratio Φ variation between 0.4 and 1.0 at ambient conditions ($T_u = 300\,\mathrm{K}$; $p = 1\,\mathrm{atm}$). Additionally, pressure variations between 1 atm and 20 atm have been evaluated at $\Phi = 0.5$ for the preheating temperatures $T_u = 300\,\mathrm{K}$, $T_u = 500\,\mathrm{K}$ and $T_u = 700\,\mathrm{K}$. Additionally, Ammonia (NH_3) at varying pre-cracking ratios for two equivalence ratios and ambient conditions is considered. Lastly, methane-hydrogen ($CH_4 - H_2$) mixtures are investigated at varying blending ratios. In the ammonia-hydrogen cases, the fuel composition is determined by the hydrogen mole fraction X_{H_2} and the following cracking ratio: $X_{N_2} = X_{H_2}/3$; $X_{NH_3} = 1 - 4/3X_{H_2}$. The complete parameter range is displayed in Tab. 1. Besides the operating conditions, mixture characteristics and flame properties of corresponding one-dimensional freely propagating flames are included, which are computed using Cantera [27].

For all configurations, reference simulations of the configuration shown in Fig. 2 are performed including the domain size variation. This adds up to $23 \cdot 9 = 207$ DNS for the model parameterization. Similar to Berger et al. [3], a normalization strategy considering the effective Lewis number Le_{eff}, Zel'dovich number Ze and thermal expansion ratio σ is applied.

The effective Lewis number Le_{eff} for fuel-lean conditions is defined as

$$Le_{\mathrm{eff}} = \frac{Le_{\mathrm{ox}} + \mathscr{A} \cdot Le_{\mathrm{f}}}{1 + \mathscr{A} \cdot Le_{\mathrm{f}}}, \tag{5}$$

with $\mathscr{A} = 1 + Ze(1/\Phi - 1)$. According to Vance et al. [28], Le_{f} and Le_{ox} are the diffusivity weighted Lewis numbers of the fuel and oxidizer components, respectively. The Zel'dovich number Ze is defined as

$$Ze = \frac{E_{\mathrm{act}} \cdot (T_b - T_u)}{R \cdot T_b^2}, \tag{6}$$

with the unburned and burned temperature, T_u and T_b, and the ideal gas constant R [28]. The effective activation energy E_{act} is determined by

$$E_{\mathrm{act}} = -2R \frac{\partial(\rho_u s_l)}{\partial(1/T_b)}, \tag{7}$$

where the derivative is calculated by a linear regression of multiple one-dimensional flames which are diluted by small amounts of N_2. The thermal expansion ratio is given as the ratio of unburned to burned density ($\sigma = \rho_u/\rho_b$). For the model parametrization, all mentioned 207 DNS simulations are considered ensuring that the resulting model is valid for a wide range of operating conditions. The resulting normalization factor $\mathscr{C}$, which is later used in the efficiency function, is determined by a least square fit to $\langle s_c \rangle / s_l$ of the DNS data and reads

$$\mathscr{C}\,(Le_{\mathrm{eff}}, Ze, \sigma) = Le_{\mathrm{eff}}^{1.27} \cdot Ze^{-1.52} \cdot \sigma^{-0.68}. \tag{8}$$

Using this normalization factor $\mathscr{C}$, the values for β_1 and β_2 are optimized and summarized in Tab. 2. Hereby, the normalization factor $\mathscr{C}$ reflects and includes the varying strength of TD instabilities at varying operating conditions.

Finally, combining Eq. (8) and Eq. (4) in Eq. (3), $\langle s_c \rangle / s_l$ can be predicted for arbitrary mixtures, operating conditions and dominating instability length scales leading to a first general formulation of the efficiency function for TD instabilities.

In Fig. 5, the model prediction $\langle s_{c,\mathrm{model}} \rangle$ is compared to the consumption speed of the reference DNS. Considering the large parameter space including varying domain sizes, multiple

TABLE 2: MODEL COEFFICIENCTS USED IN EQ. (4)

regime	β_1	β_2
$\Delta/\lambda_{\text{crit}} < 1$	0	0
$\Delta/\lambda_{\text{crit}} < 4$	$3.38 \cdot 10^{-3}$	−0.27
$\Delta/\lambda_{\text{crit}} > 4$	$1.17 \cdot 10^{-3}$	0.51

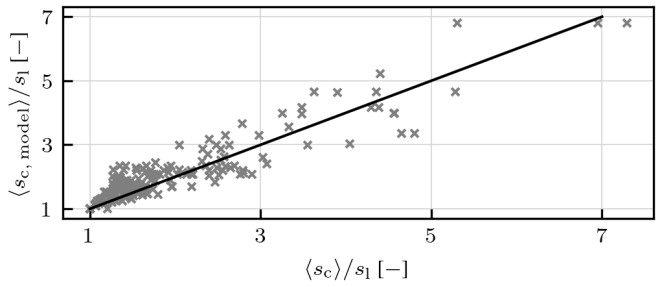

FIGURE 5: COMPARISON OF $\langle s_{c,\text{model}}\rangle/s_l$ PREDICTED BY THE MODEL TO $\langle s_c\rangle/s_l$ DETERMINED BY THE REFERENCE DNS FOR ALL CONDITIONS OF TAB. 1.

operating conditions, and varying fuel mixtures, the model can accurately predict the laminar flame consumption speed. For the entire parameter space, including all conditions from Tab. 1, the model predicts $\langle s_c\rangle/s_l$ with an average error of 12 %.

3.4 Model evaluation in a simplified configuration

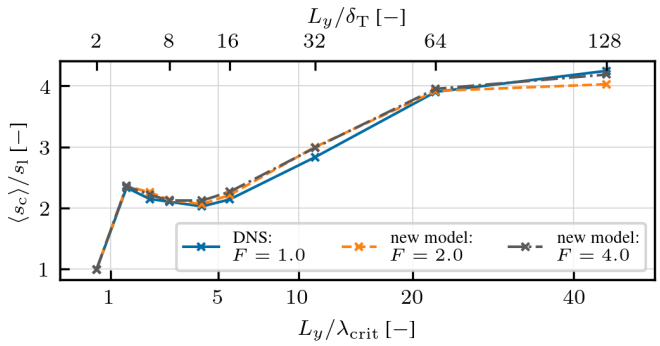

FIGURE 6: FULLY COUPLED MODEL EVALUATION SHOWN BY THE AVERAGED FUEL CONSUMPTION SPEED INCREASE $\langle s_c\rangle/s_l$ PLOTTED FOR VARYING DOMAIN SIZES L_y AND THICKENING FACTORS F AT THE SAME CONDITIONS AS SHOWN IN FIG. 4.

To further evaluate the proposed model, the model is implemented and tested in a fully coupled *a-posteriori* manner using the configuration shown in Fig. 2. The mixture-dependent quantities Le_{eff}, Ze, σ and λ_{crit} are computed prior to the simulations for the given conditions (cf. Tab 1). The result of the fully coupled model evaluation is shown exemplary for a single condition in Fig. 6 over varying domain sizes and for two thickening factors. The DNS ($F = 1$) is also shown for reference. Similar trends are observed for the other conditions which are omitted here for brevity. As an example, the simulation with $F = 4$ and a domain size of $L_y = 128\delta_T$ showed an error of over 40% without a model (Fig. 4) which decreased to 1.4% by using the proposed efficiency function (Fig. 6). For $F = 2$ and $L_y = 128\delta_T$, the error is reduced from 30% to 5%. This demonstrates that the proposed model significantly improves the prediction of the flame speed compared to the standard model.

4. MODEL APPLICATION TO TURBULENT FLAMES

In this section, the proposed model is extended and applied to turbulent conditions. First, the length scale required for the extended ATF model is derived for turbulent conditions. Second, the model is evaluated using reference data from DNS of turbulent jet flames.

4.1 Model transfer to turbulent conditions

The model extension proposed in Sec. 3 bases on the scaling of flame characteristics with the thickening factor. For this, a length scale Δ is defined as the upper length scale which can be understood as the largest instability size which is determined as the minimum of the largest intrinsic length scale and an externally determined length scale. For the laminar configuration, this length scale has been shown to be the domain size L_y (cf. Sec. 3). For the turbulent cases, this length scale is estimated to be a length scale on which the resolved flame and turbulent structures interact. According to the derivation of the state-of-the-art efficiency functions [12, 29], this length scale is estimated as $10\Delta_x$, where Δ_x is the local grid size. Therefore, similar to the well-established turbulent efficiency function, our proposed efficiency function in Eq. (3) uses $10\Delta_x$ as external length scale so that $\Delta = \min\left(L_{\text{cell,max}}, 10\Delta_x\right)$. This definition is advantageous since it facilitates the implementation of the efficiency function into existing solvers exploiting the same input parameters as the turbulent efficiency function. Besides the enhanced flame speed due to TD instabilities, the turbulent wrinkling needs to be considered. For this, the mentioned formulation of Charlette et al. [12] is taken as E_{turb}. The combination of the turbulent and intrinsic flame wrinkling is linearly superimposed so that the overall efficiency function E is defined as:

$$E = E_{\text{turb}} \cdot E_{\text{TD}}, \tag{9}$$

where E_{TD} is the proposed model from Eq. (3) in Sec. 3 using the length scale $\Delta = \min\left(L_{\text{cell,max}}, 10\Delta_x\right)$. Non-linear interaction of the turbulent (E_{turb}) and flame intrinsic wrinkling (E_{TD}) is to be investigated in future studies. Here, especially the synergistic interaction of turbulence and TD instabilities is of interest. For model evaluation, the efficiency function is implemented according to Eq. (9) and Eq. (2) in OpenFOAM using the model parameter given in Sec. 3.

The ATF approach is known for changing the flame dynamics in highly strained flows altering the turbulent flame speed. Several options to correct this are available in the literature [14, 17]. However, these approaches are either only valid for tabulated chemistry [14] or single-step chemistry [17]. Therefore, the well-established turbulent efficiency function by Charlette et al. [12] is considered even though it does not account for the altered flame dynamics of the thickened flame in highly strained regions.

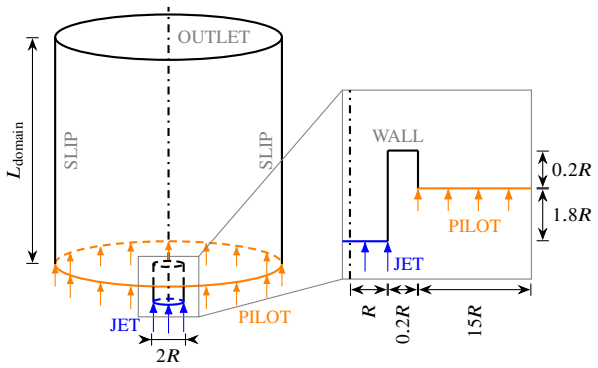

FIGURE 7: SCHEMATIC OF THE COMPUTATIONAL DOMAIN OF THE TURBULENT JET FLAME CONFIGURATION.

This disadvantage of the turbulent efficiency function needs to be considered during model evaluation. Nevertheless, this work focuses on developing a TD instability-aware model extension that can be interchangeably used with other turbulent efficiency functions.

4.2 Model evaluation in turbulent jet flames

For the model evaluation, multiple Direct Numerical Simulations (DNS) and Large-Eddy Simulations (LES) of a turbulent jet flame under varying operating conditions are conducted. The configuration is shown in Fig. 7 and consists of a turbulent jet of fresh gases and a pilot with burned products of the corresponding jet mixture. The radius of the jet R is set to $R = 4.5\,\text{mm}$. An adiabatic wall with no-slip conditions for the velocity separates the jet from the pilot. The domain size is deliberately set large enough to ensure that the outlet and sides do not interfere with the flame. A constant velocity of $15\%\,u_{\text{bulk}}$ is set at the pilot, where u_{bulk} is the bulk velocity of the jet.

Four different operating conditions are investigated according to Tab. 3 resembling a subset of conditions of Sec. 3. Hereby, all operating conditions are operated with mixtures prone to TD instabilities. Besides an ambient hydrogen case serving as a reference, a case with preheated fresh gas is simulated. The Reynolds number Re is set to $20,000$ for these cases. Additionally, an ammonia-hydrogen-nitrogen mixture representing partially cracked ammonia and a hydrogen-methane mixture are investigated at $Re \approx 12,000$.

The DNS are calculated using the spectral element method code nekRS [30] in combination with the chemistry plugin nekCRF [31] for low Mach number reacting flows employing a 7th-order spatial discretization and 3rd-order temporal discretization. Transport is modeled using the mixture-averaged approach, neglecting thermo-diffusion. The inlet pipe is prolonged to $16R$ and velocity recycling is employed for the DNS cases to ensure fully developed turbulence in the jet. The DNS are performed utilizing nekCRF's GPU capabilities since the meshes encompass close to two billion cells in the cases with $Re = 20,000$.

For each DNS operating condition, four LES are computed using OpenFOAM. Here, the velocity inflow profiles for the jet are pre-computed using time-resolved DNS data of pipe flows at the corresponding condition. The spatial resolution is varied leading to varying modeling efforts. The thickening factor is set so that the flame front is always resolved by 10 grid points employing a grid-adaptive thickening approach [11]. Subsequently, the average thickening factors for the finer meshes are $F \approx 4$, while the coarser meshes lead to an average thickening factor of $F \approx 8$. To evaluate the proposed model, the LES are computed with the state-of-the-art model by Charlette et al. [12] and compared to LES computed using the new model extension from this study. The corresponding meshes are summarized in Tab. 3 showing a significant reduction of spatial resolution requirements compared to the DNS. A flame sensor based on the Y_{H_2O} mass fraction is used to only apply the thickening to the reaction zone. In total, four DNS and 16 LES of the configuration at varying conditions are calculated to provide a comprehensive model evaluation.

The flames are shown in Fig. 8, where the first column corresponds to the DNS. The second and fourth columns show the LES using only the state-of-the-art turbulent efficiency function E_{turb} while the third and last columns display the LES with the proposed efficiency function from Eq. (9). Each row corresponds to an operating condition from Tab. 3. For each simulation, an instantaneous snapshot of the Y_{OH} mass fraction is shown on the left and the time-averaged Y_{HO_2} profile on the right, providing an estimate of the flame height.

The contours in Fig. 8 highlight that the state-of-the-art model, which accounts only for turbulent flame wrinkling, substantially underestimates flame speed, leading to overestimated flame length. Although increasing the spatial resolution increases the resolved flame wrinkling, this does not result in a significant improvement in the flame speed prediction. Including TD instabilities in the efficiency function as done in columns three and five results in a more accurate flame speed prediction for all operating conditions and for both (coarse and fine) resolutions. As expected, including the TD efficiency function E_{TD} does not increase flame wrinkling but improves the global fuel consumption speed prediction. Although the flame in the coarse LES shows significantly less wrinkling, the model predicts similar flame heights as in the fine LES cases indicating that the chosen length scale Δ_x is suitable for varying mesh resolutions.

TABLE 3: OPERATING CONDITIONS OF THE TURBULENT JET FLAME. FOR EACH CONDITION A DNS AND FOUR LES ARE COMPUTED.

fuel	$X_{H_2,\text{fuel}}$ [%]	Φ [−]	p [atm]	T_u [K]	s_l [cm s^{-1}]	δ_T [µm]	Re [−]	u_{bulk} [m s^{-1}]	$N_{\text{total, DNS}}$ [billion]	$N_{\text{total, LES,fine}}$ [million]	$N_{\text{total, LES,coarse}}$ [million]
H2	1	0.50	1.0	300	53.13	427	$2{\cdot}10^4$	42.5	1.9	8.5	1.1
H2	1	0.50	1.0	500	201.16	434	$2{\cdot}10^4$	102.0	1.9	8.5	1.1
NH3-H2-N2	0.6	0.70	1.0	300	49.63	436	$1.2{\cdot}10^4$	25.0	0.9	8.5	1.1
CH4-H2	0.8	0.60	1.0	300	35.93	479	$1.2{\cdot}10^4$	25.0	0.9	8.5	1.1

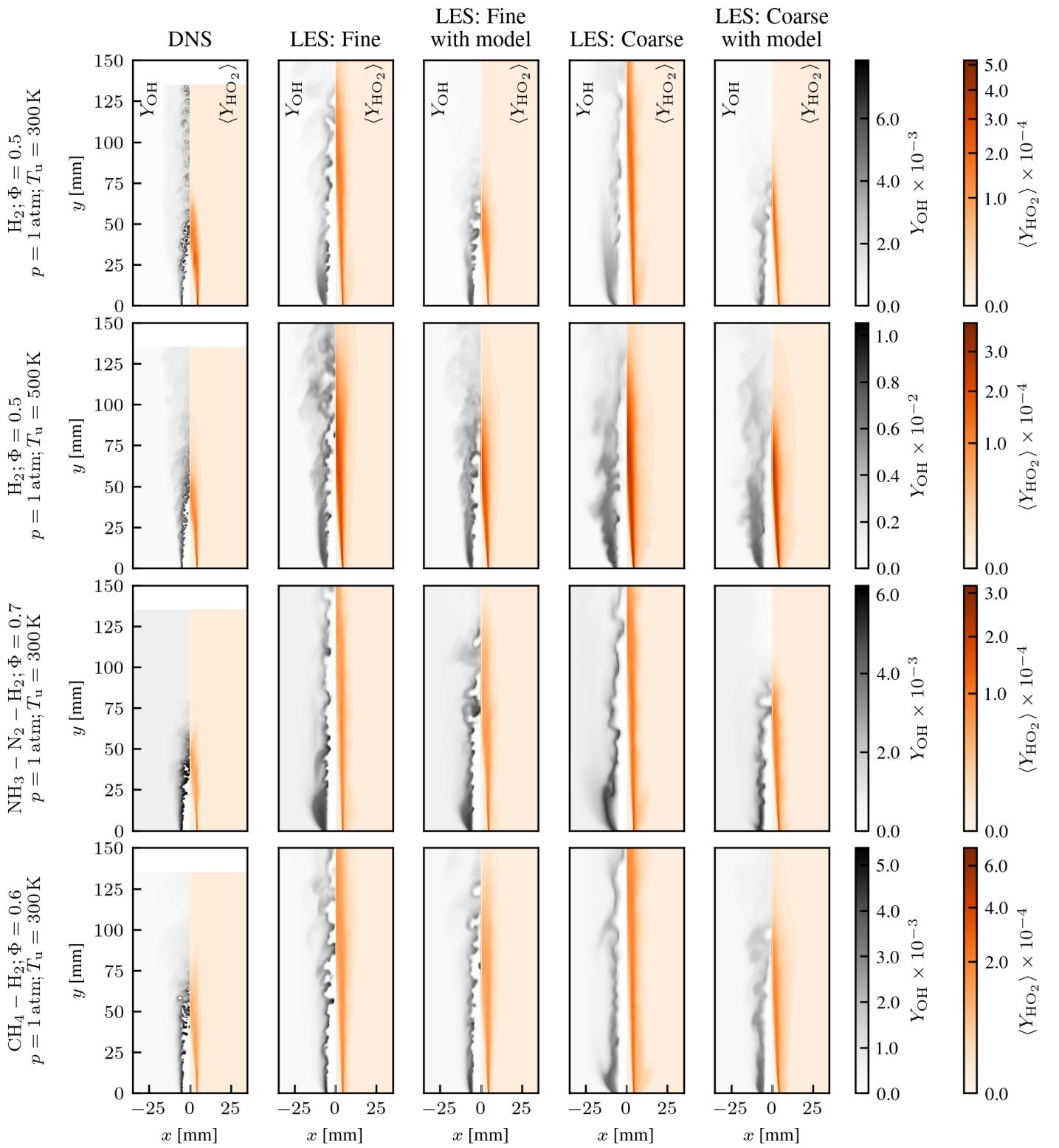

FIGURE 8: OVERVIEW OF THE TURBULENT JET FLAME SIMULATIONS. INSTANTANEOUS SNAPSHOTS OF THE Y_{OH} MASS FRACTION ARE SHOWN ON THE LEFT WHILE THE TIME-AVERAGED $\langle Y_{HO_2} \rangle$ MASS FRACTION IS DISPLAYED ON THE RIGHT OF EACH CONTOUR. EACH ROW CORRESPONDS TO AN OPERATING CONDITION LISTED IN TAB. 3. THE COLUMNS ARE (FROM LEFT TO RIGHT) DNS, FINE LES WITH THE STATE-OF-THE-ART MODEL, FINE LES WITH MODEL EXTENSION (EQ. (9)), FOLLOWED BY THE COARSE LES RESULTS WITH AND WITHOUT THE MODEL EXTENSION. ONLY A PART OF THE DOMAIN IS SHOWN.

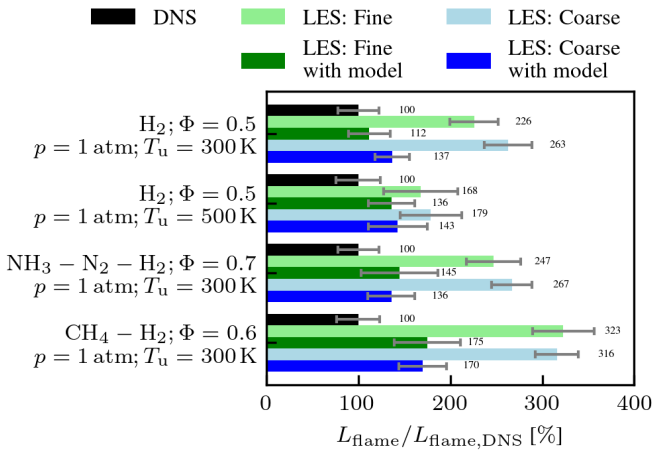

FIGURE 9: FLAME LENGTHS FOR ALL OPERATING CONDITIONS ARE SHOWN RELATIVE TO THE LENGTH OF THE RESPECTIVE DNS. FLAME LENGTHS ARE DETERMINED BY THE MAXIMUM TIME-AVERAGED $\langle Y_{HO_2} \rangle$ MASS FRACTION. ERROR-BARS INDICATE 50 % OF THE MAXIMUM$\langle Y_{HO_2} \rangle$.

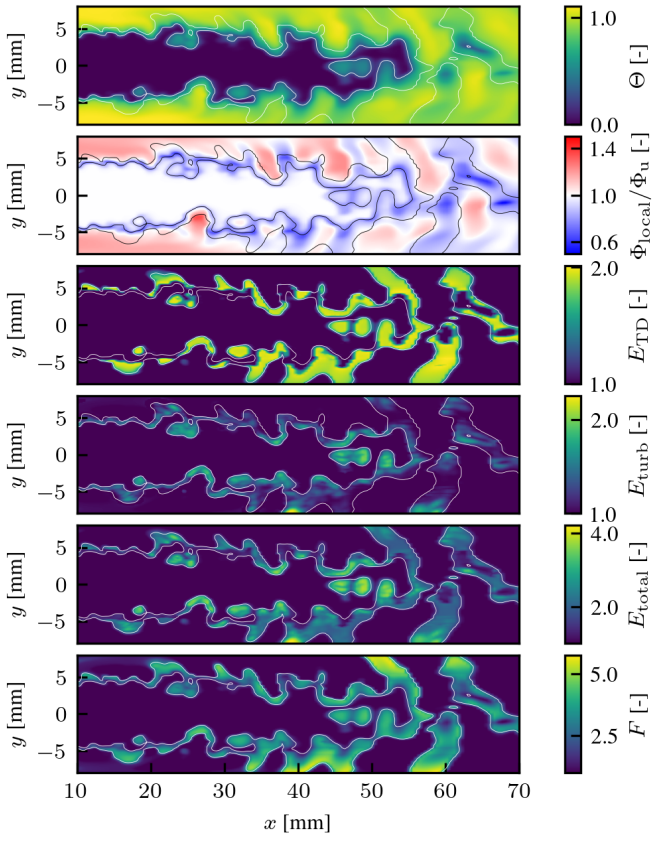

FIGURE 10: CLOSE UP CONTOUR PLOTS OF THE LES AT AMBIENT CONDITIONS WITH PURE H_2. THE SHOWN QUANTITIES ARE NORMALIZED TEMPERATURE $\Theta = (T - T_u)/(T_{ad} - T_u)$, NORMALIZED LOCAL EQUIVALENCE RATIO Φ_{local}/Φ_u, EFFICIENCY FUNCTIONS E_{TD}, E_{turb}, $E_{total} = E_{TD} \cdot E_{turb}$ AND THICKENING FACTOR F.

The model's performance is evaluated by comparing the flame heights predicted by the LES to those found in the DNS data. The flame height is determined by the time-averaged mass fraction $\langle Y_{HO_2} \rangle$, which is found to be a good flame marker. The flames are averaged until no visible changes in the flame position are apparent. The flame height is determined by the maximum time-averaged $\langle Y_{HO_2} \rangle$ mass fraction at the center of the domain. The resulting flame heights are summarized relative to the DNS flame heights in Fig. 9. The model significantly improves the flame height prediction indicating a more accurate representation of the global flame speed. Specifically, for pure hydrogen, the flame length errors are reduced from approximately 200 % to around 30 %, while slightly higher errors are observed for hydrogen-enriched mixtures. Note that the state-of-the-art model predicts turbulent flame speed more accurately for the preheated hydrogen case compared to other operating conditions, as TD instabilities are less pronounced with increased preheating – an effect correctly captured by the developed model extension. Further differences in the flame length, as seen in the methane-hydrogen case, could also be attributed to the underlying turbulent efficiency function E_{turb} necessitating further development of modeling the flame's response to turbulence by, e.g., including stretch effects for detailed chemistry. Another uncertainty is the different numerical treatment of OpenFOAM compared to the high-order DNS code which could contribute to the mismatched flame length between LES and DNS through numerical dissipation.

Lastly, the local effect and characteristics of the introduced efficiency function are discussed. Therefore, closeup contours of the fine LES with the improved efficiency function (Eq. (9)) at ambient conditions are shown in Fig. 10. All contours include the flame sensor as white isolines for easier identification of the flame front. The normalized temperature Θ and normalized local equivalence ratio $\Phi_{\mathrm{local}}/\Phi_u$ show the effect of hydrogen's characteristics leading to local mixture stratification ($\Phi_{\mathrm{local}}/\Phi_u \neq 1$) and super-adiabatic temperatures ($\Theta > 1$) in locally richer regions in the turbulent flame. Even though the flame front is strongly influenced by turbulent structures, super-adiabatic temperatures, similar to the laminar configuration (Fig. 3), are not suppressed. Additionally, since the flame is thickened by F, the impact of non-resolved wrinkling and mixture stratification needs to be included in the subgrid modeling underlining the importance of the new efficiency function E_{TD}. Hereby, E_{TD} takes similar values as the turbulent efficiency function E_{turb}. The superposition of E_{TD} and E_{turb} is represented by E_{total} demonstrating that the efficiency function increases the reaction rates, especially in regions of positive curvature. Overall, the proposed model enhances the prediction of global turbulent flame speeds across various conditions and fuels while preserving the flame structure, including key features such as mixture stratification and super-adiabatic temperatures.

5. CONCLUSION

This study introduces an enhanced Artificially Thickened Flame (ATF) model tailored for lean premixed hydrogen and hydrogen-enriched flames, focusing on improved predictions under gas turbine-relevant conditions. The key steps and findings are as follows:

1. Over 200 Direct Numerical Simulations (DNS) of laminar thermo-diffusive (TD) unstable flames were conducted under conditions relevant to gas turbines, including high preheating temperatures and elevated pressures.
2. The resulting database was extensively analyzed to develop a general TD sub-grid model tailored for these scenarios.
3. The subsequently developed model was validated against a simplified configuration, showing excellent agreement with a reference DNS, with errors below 2 %. In contrast, neglecting the model resulted in errors exceeding 40 %.
4. The model was integrated into Large Eddy Simulations (LES) and applied to four turbulent jet flames with varying mixtures, and temperatures. LES results on both fine and coarse grids were compared to high-fidelity DNS data comprising close to two billion cells. The novel sub-grid model demonstrated substantial improvements in flame speed predictions compared to state-of-the-art approaches across all four cases.
5. Remarkably, the model captures phenomena associated with instabilities, such as mixture stratification and super-adiabatic temperatures, showcasing its robustness and versatility.

Future research aims to explore non-linear interactions between turbulence and thermodiffusive instabilities, with the potential to even further enhance the agreement between model predictions and reference data.

ACKNOWLEDGMENTS

This research has been funded by the German Federal Ministry for Education and Research under grant 03SF0640B. The authors gratefully acknowledge the computing time provided to them at the NHR Center NHR4CES at RWTH Aachen University (project number p0020682). This is funded by the Federal Ministry of Education and Research, and the state governments participating on the basis of the resolutions of the GWK for national high performance computing at universities (www.nhr-verein.de/unsere-partner). The research leading to these results has received funding from EuroHPC within the Inno4Scale project. The Inno4scale project has received funding from the European High-Performance Computing Joint Undertaking (JU) under Grant Agreement No 101118139. The JU receives support from the European Union's Horizon Europe Programme. The authors gratefully acknowledge the Gauss Centre for Supercomputing e.V. (www.gauss-centre.eu) for funding this project by providing computing time on the GCS Supercomputer JUWELS at Jülich Supercomputing Centre (JSC).

REFERENCES

[1] Pitsch, H. "The transition to sustainable combustion: Hydrogen- and carbon-based future fuels and methods for dealing with their challenges." *Proceedings of the Combustion Institute* Vol. 40 No. 1-4 (2024): p. 105638. DOI 10.1016/j.proci.2024.105638.

[2] Berger, L., Kleinheinz, K., Attili, A. and Pitsch, H. "Characteristic patterns of thermodiffusively unstable premixed lean hydrogen flames." *Proceedings of the Combustion Institute* Vol. 37 No. 2 (2019): pp. 1879–1886. DOI 10.1016/j.proci.2018.06.072.

[3] Berger, L., Attili, A. and Pitsch, H. "Intrinsic instabilities in premixed hydrogen flames: parametric variation of pressure, equivalence ratio, and temperature. Part 2 – Non-linear regime and flame speed enhancement." *Combustion and Flame* Vol. 240 (2022): p. 111936. DOI 10.1016/j.combustflame.2021.111936.

[4] Berger, L., Attili, A. and Pitsch, H. "Synergistic interactions of thermodiffusive instabilities and turbulence in lean hydrogen flames." *Combustion and Flame* Vol. 244 (2022): p. 112254. DOI 10.1016/j.combustflame.2022.112254.

[5] Schuh, V., Hasse, C. and Nicolai, H. "An extension of the artificially thickened flame approach for premixed hydrogen flames with intrinsic instabilities." *Proceedings of the Combustion Institute* Vol. 40 No. 1-4 (2024): p. 105673. DOI 10.1016/j.proci.2024.105673.

[6] Kadowaki, S. and Hasegawa, T. "Numerical simulation of dynamics of premixed flames: flame instability and vortex–flame interaction." *Progress in Energy and Combustion Science* Vol. 31 No. 3 (2005): pp. 193–241. DOI 10.1016/j.pecs.2005.01.001.

[7] Altantzis, C., Frouzakis, C. E., Tomboulides, A. G., Matalon, M. and Boulouchos, K. "Hydrodynamic and thermodiffusive instability effects on the evolution of laminar planar lean premixed hydrogen flames." *Journal of Fluid Mechanics* Vol. 700 (2012): pp. 329–361. DOI 10.1017/jfm.2012.136.

[8] Creta, F., Lapenna, P. E., Lamioni, R., Fogla, N. and Matalon, M. "Propagation of premixed flames in the presence of Darrieus–Landau and thermal diffusive instabilities." *Combustion and Flame* Vol. 216 (2020): pp. 256–270. DOI 10.1016/j.combustflame.2020.02.030.

[9] Lapenna, P. E., Lamioni, R. and Creta, F. "Subgrid modeling of intrinsic instabilities in premixed flame propagation." *Proceedings of the Combustion Institute* Vol. 38 No. 2 (2021): pp. 2001–2011. DOI 10.1016/j.proci.2020.06.192.

[10] O'Rourke, P. J. and Bracco, F. V. "Two scaling transformations for the numerical computation of multidimensional unsteady laminar flames." *Journal of Computational Physics* Vol. 33 No. 2 (1979): pp. 185–203. DOI 10.1016/0021-9991(79)90015-9.

[11] Kuenne, G., Seffrin, F., Fuest, F., Stahler, T., Ketelheun, A., Geyer, D., Janicka, J. and Dreizler, A. "Experimental and numerical analysis of a lean premixed stratified burner using 1D Raman/Rayleigh scattering and large eddy simulation." *Combustion and Flame* Vol. 159 No. 8 (2012): pp. 2669–2689. DOI 10.1016/j.combustflame.2012.02.010.

[12] Charlette, F., Meneveau, C. and Veynante, D. "A power-law flame wrinkling model for LES of premixed turbulent combustion Part I: non-dynamic formulation and initial tests." *Combustion and Flame* Vol. 131 No. 1-2 (2002): pp. 159–180. DOI 10.1016/S0010-2180(02)00400-5.

[13] Nicolai, H., Dressler, L., Janicka, J. and Hasse, C. "Assessing the importance of differential diffusion in stratified hydrogen–methane flames using extended flamelet tabulation approaches." *Physics of Fluids* Vol. 34 No. 8 (2022): p. 085118. DOI 10.1063/5.0102675.

[14] Popp, S., Kuenne, G., Janicka, J. and Hasse, C. "An extended artificial thickening approach for strained premixed flames." *Combustion and Flame* Vol. 206 (2019): pp. 252–265. DOI 10.1016/j.combustflame.2019.04.047.

[15] Poncet, S., Mehl, C., Truffin, K. and Colin, O. "A Thickened Flame Model adaptation to weakly stretched flames for non-unity Lewis number mixtures." *Combustion and Flame* Vol. 270 (2024): p. 113758. DOI 10.1016/j.combustflame.2024.113758.

[16] Hok, J.-J., Dounia, O., Detomaso, N., Jaravel, T., Douasbin, Q. and Vermorel, O. "A modeling strategy for the Thickened Flame simulation of propagating lean hydrogen–air flames." *International Journal of Hydrogen Energy* Vol. 78 (2024): pp. 1133–1141. DOI 10.1016/j.ijhydene.2024.06.298.

[17] Detomaso, N., Hok, J.-J., Dounia, O., Laera, D. and Poinsot, T. "A generalization of the Thickened Flame model for stretched flames." *Combustion and Flame* Vol. 258 (2023): p. 113080. DOI 10.1016/j.combustflame.2023.113080.

[18] Gaucherand, J., Schulze-Netzer, C., Laera, D. and Poinsot, T. "A subgrid-scale model to account for thermo-diffusive effects in artificially thickened LES models for lean turbulent premixed ammonia/hydrogen flames." *Proceedings of the Combustion Institute* Vol. 40 No. 1-4 (2024): p. 105198. DOI 10.1016/j.proci.2024.105198.

[19] Böttler, H., Kaddar, D., Karpowski, T. J. P., Ferraro, F., Scholtissek, A., Nicolai, H. and Hasse, C. "Can flamelet manifolds capture the interactions of thermo-diffusive instabilities and turbulence in lean hydrogen flames?—An a-priori analysis." *International Journal of Hydrogen Energy* Vol. 56 (2024): pp. 1397–1407. DOI 10.1016/j.ijhydene.2023.12.193.

[20] Esclapez, L., Day, M., Bell, J., Felden, A., Gilet, C., Grout, R., De Frahan, M. H., Motheau, E., Nonaka, A., Owen, L., Perry, B., Rood, J., Wimer, N. and Zhang, W. "PeleLMeX: an AMR Low Mach Number Reactive FlowSimulation Code without level sub-cycling." *Journal of Open Source Software* Vol. 8 No. 90 (2023): p. 5450. DOI 10.21105/joss.05450.

[21] Kee, R. J., Coltrin, M. E., Glarborg, P. and Zhu, H. *Chemically Reacting Flow: Theory, Modeling, and Simulation*, 1st ed. Wiley (2017). DOI 10.1002/9781119186304.

[22] Howarth, T.L., Day, M.S., Pitsch, H. and Aspden, A.J. "Thermal diffusion, exhaust gas recirculation and blending effects on lean premixed hydrogen flames." *Proceedings of the Combustion Institute* Vol. 40 No. 1-4 (2024): p. 105429. DOI 10.1016/j.proci.2024.105429.

[23] Burke, M. P., Chaos, M., Ju, Y., Dryer, F. L. and Klippenstein, S. J. "Comprehensive H_2/O_2 kinetic model for high-pressure combustion: Comprehensive H_2/O_2 Kinetic Model for High-Pressure Combustion." *International Journal of Chemical Kinetics* Vol. 44 No. 7 (2012): pp. 444–474. DOI 10.1002/kin.20603.

[24] Stagni, A., Frassoldati, A., Cuoci, A., Faravelli, T. and Ranzi, E. "Skeletal mechanism reduction through species-targeted sensitivity analysis." *Combustion and Flame* Vol. 163 (2016): pp. 382–393. DOI 10.1016/j.combustflame.2015.10.013.

[25] Stagni, A., Arunthanayothin, S., Dehue, M., Herbinet, O., Battin-Leclerc, F., Bréquigny, P., Mounaïm-Rousselle, C. and Faravelli, T. "Low- and intermediate-temperature ammonia/hydrogen oxidation in a flow reactor: Experiments and a wide-range kinetic modeling." *Chemical Engineering Journal* Vol. 471 (2023): p. 144577. DOI 10.1016/j.cej.2023.144577.

[26] Smooke, M. D. and Giovangigli, V. "Formulation of the premixed and nonpremixed test problems." *Reduced Kinetic Mechanisms and Asymptotic Approximations for Methane-Air Flames* Vol. 384 (1991): pp. 1–28. DOI 10.1007/BFb0035363.

[27] Goodwin, D. G., Moffat, H. K., Schoegl, I., Speth, R. L. and Weber, B. W. "Cantera: An Object-oriented Software Toolkit for Chemical Kinetics, Thermodynamics, and Transport Processes." (2023). DOI 10.5281/zenodo.8137090.

[28] Vance, F. H., Nicolai, H. and Hasse, C. "A numerical investigation into the stabilization of hydrogen enriched n-dodecane premixed flames." *International Journal of Hydrogen Energy* Vol. 56 (2024): pp. 611–620. DOI 10.1016/j.ijhydene.2023.12.219.

[29] Colin, O., Ducros, F., Veynante, D. and Poinsot, T. "A thickened flame model for large eddy simulations of turbulent premixed combustion." *Physics of Fluids* Vol. 12 No. 7 (2000): pp. 1843–1863. DOI 10.1063/1.870436.

[30] Fischer, P., Kerkemeier, S., Min, M., Lan, Y.-H., Phillips, M., Rathnayake, T., Merzari, E., Tomboulides, A., Karakus, A., Chalmers, N. and Warburton, T. "NekRS, a GPU-accelerated spectral element Navier–Stokes solver." *Parallel Computing* Vol. 114 (2022): p. 102982. DOI 10.1016/j.parco.2022.102982.

[31] Kerkemeier, S., Frouzakis, C. E., Tomboulides, A. G., Fischer, P. and Bode, M. "nekCRF: A next generation high-order reactive low Mach flow solver for direct numerical simulations." (2024). DOI 10.48550/arXiv.2409.06404.